

Article

Positive Effect of Ce Modification on Low-Temperature NH₃-SCR Performance and Hydrothermal Stability over Cu-SSZ-16 Catalysts

Yuqian Liang¹, Rui Li², Ruicong Liang¹, Zhanhong Li¹, Xiangqiong Jiang¹ and Jiuxing Jiang^{1,3,*} 

¹ MOE Key Laboratory of Bioinorganic and Synthetic Chemistry, School of Chemistry, Sun Yat-sen University, Guangzhou 510275, China

² State Key Laboratory of Green Chemical Engineering and Industrial Catalysis, Sinopec Shanghai Research Institute of Petrochemical Technology, Shanghai 201208, China

³ Jiangxi Provincial Key Laboratory of Low-Carbon Solid Waste Recycling Technology, School of Geography and Environmental Engineering, Gannan Normal University, Ganzhou 341000, China

* Correspondence: jiangjiux@mail.sysu.edu.cn

Abstract: Cu-exchanged SSZ-16 zeolite catalysts exhibit outstanding NH₃-SCR activity, but their catalytic performance after hydrothermal treatments is not ideal. In order to improve the hydrothermal stability of Cu-SSZ-16, CuCe_x-SSZ-16 series catalysts were prepared via an ion exchange process, and the effect of Ce modification on the hydrothermal stability was investigated. In addition, increasing Ce contents significantly improved the hydrothermal stability, and CuCe_{0.87}-SSZ-16 showed the best hydrothermal stability. The effects of adding Ce to active species and the AFX framework were studied by various characterization measurements. The ²⁷Al MAS NMR results reveal that Ce modification can strengthen the structural stability of the CuCe_x-SSZ-16 catalysts. Furthermore, the combined results of XPS, H₂-TPR, and in situ DRIFTS confirm that the introduction of Ce markedly increases the active Cu²⁺-2Z species, contributing to the remarkable hydrothermal stability.

Keywords: Cu-SSZ-16; Ce content; NH₃-SCR; low temperature; hydrothermal stability



Citation: Liang, Y.; Li, R.; Liang, R.; Li, Z.; Jiang, X.; Jiang, J. Positive Effect of Ce Modification on Low-Temperature NH₃-SCR Performance and Hydrothermal Stability over Cu-SSZ-16 Catalysts. *Catalysts* **2023**, *13*, 742. <https://doi.org/10.3390/catal13040742>

Academic Editors: De Fang and Yun Zheng

Received: 28 February 2023

Revised: 6 April 2023

Accepted: 7 April 2023

Published: 13 April 2023



Copyright: © 2023 by the authors. Licensee MDPI, Basel, Switzerland. This article is an open access article distributed under the terms and conditions of the Creative Commons Attribution (CC BY) license (<https://creativecommons.org/licenses/by/4.0/>).

1. Introduction

Nitrogen oxides (NO_x) have been identified as a significant air pollutant that causes a large number of environmental issues and harms human health [1,2]. The primary sources of NO_x in cities are emissions from power plants and automobile engines, of which diesel engines account for a large proportion [3]. Consequently, the control of NO_x emitted from diesel engines is essential. Ammonia-selective catalytic reduction (NH₃-SCR) is regarded as a highly efficient denitration technique because of its excellent deNO_x performance [4]. Nowadays, many Cu-exchanged zeolites have been widely considered due to their outstanding deNO_x activity and hydrothermal stability. Among them, Cu-exchanged CHA, AEI, SFW, and AFX catalysts have been extensively investigated in previous studies [5–10]. However, severe high-temperature hydrothermal treatments destroy the skeleton of zeolite and reduce the active species, causing the loss of NH₃-SCR activity.

The effect of Cu species in Cu-exchanged zeolites has been extensively studied [11–13]. It is universally acknowledged that Cu²⁺ species, including Cu²⁺-2Z and [Cu(OH)]⁺-Z (where Z stands for a framework negative charge), provide active sites for the NH₃-SCR reaction [14]. Cu²⁺-2Z species refer to Cu²⁺ located in the 6-ring, while the Cu²⁺ sites residing in the 8-ring are recorded as [Cu(OH)]⁺-Z [15,16]. The two kinds of Cu²⁺ species behave differently under hydrothermal treatments. Cu²⁺-2Z species are considered relatively stable active sites with higher hydrothermal stability, contributing to NO_x removal [4,17–20]. However, [Cu(OH)]⁺-Z is more beneficial to low-temperature (<300 °C) deNO_x reactions, though it may transform to Cu²⁺-2Z or CuO_x clusters with increasing temperature [21,22]. The CuO_x clusters might block the pores of zeolites, leading to a reduction in NH₃-SCR activity [23].

The Cu-SSZ-16 with an AFX structure exhibits remarkable NH₃-SCR performance, but its low-temperature activity is reduced to varying degrees after hydrothermal treatments at different temperatures [10]. Since hydrothermal stability is vital to the application of catalysts, the improvement of zeolite catalysts should also focus on hydrothermal stability. According to the literature, hydrothermal deactivation is mainly caused by a decrease in the active Cu²⁺ species and the structural instability resulting from skeleton dealumination, which can be alleviated by some means, for example, by introducing some elements [24–26]. Previous studies have demonstrated that introducing Ce to Cu-exchanged zeolites could ameliorate their hydrothermal stability. Wang et al. proposed that the addition of Ce could greatly promote the catalytic activity and hydrothermal stability of Cu-SSZ-39 catalysts [27]. Mao et al. perceived that the higher hydrothermal stability of Cu-Ce/SAPO-34 might be obtained by increasing the additional content of Ce, for Ce doping could prevent hydrothermal treatments from causing damage to the partial pore structure and a reduction in the catalyst's crystallinity [28]. Deng et al. found that Ce doping could improve the hydrothermal stability of Cu/SSZ-13 catalysts, owing to the increased framework aluminum and the more stable Cu sites [29]. Jiang and co-workers reported that the introduction of Ce might stabilize the zeolite skeleton and increase the active Cu²⁺ species, leading to the excellent hydrothermal stability of CeCu-SSZ-52 [30]. However, developing new catalysts with outstanding catalytic activity and hydrothermal stability is still crucial. Cu-SSZ-16 catalysts show superior deNO_x activity, but their hydrothermal stability needs to be increased to allow commercial application.

In this study, CuCe_x-SSZ-16 series catalysts ($x = 0.77$ wt.% and 0.87 wt.%) were synthesized to study their low-temperature NH₃-SCR catalytic activity as well as their hydrothermal stability. Various characterization measurements such as XRD, ²⁷Al MAS NMR, XPS, H₂-TPR, EPR, UV-vis, and in situ DRIFTS were used to probe the influence of adding Ce to the catalysts, including the changes in the active species and zeolite framework.

2. Results and Discussion

2.1. NH₃-SCR Activity and SO₂ Resistance Test

The NO_x conversion curves of the NH₃-SCR reaction over Cu-SSZ-16-Fresh, CuCe_{0.77}-SSZ-16-Fresh, and CuCe_{0.87}-SSZ-16-Fresh (where “Fresh” represents the samples tested before the hydrothermal treatments) are displayed in Figure 1a. The NO_x reduction efficiency of Cu-SSZ-16-Fresh reaches 90% at about 215 °C and remains above 90% at 215–400 °C. Compared with Cu-SSZ-16-Fresh, CuCe_{0.77}-SSZ-16-Fresh and CuCe_{0.87}-SSZ-16-Fresh exhibit better low-temperature catalytic activity with higher NO_x conversion from 150 to 250 °C and the conversion is maintained at 95% from 250 to 400 °C. Additionally, the N₂ selectivity is slightly improved, and the selectivity of the NO₂ and N₂O byproducts declines at low temperatures (<250 °C) with the incorporation of Ce (Figure S1a–c).

In order to inquire about the changes in the hydrothermal stability with the addition of Ce, Cu-SSZ-16, CuCe_{0.77}-SSZ-16, and CuCe_{0.87}-SSZ-16 catalysts were treated at the hydrothermal temperature of 750 °C (referred to as Cu-SSZ-16-750HT, CuCe_{0.77}-SSZ-16-750HT, and CuCe_{0.87}-SSZ-16-750HT). The catalytic data in Figure 1b illustrate that the NO_x reduction efficiency of Cu-SSZ-16-750HT reaches 90% at around 265 °C, while CuCe_x-SSZ-16-750HT series catalysts achieve 90% NO_x conversion at about 240 °C. The results reveal that the NH₃-SCR activity is enhanced at low temperatures (<250 °C) after Ce is added. The N₂, NO₂, and N₂O selectivity of the Cu-SSZ-16-750HT and CuCe_x-SSZ-16-750HT series catalysts is presented in Figure S1d–f. The N₂ selectivity of Cu-SSZ-16-750HT decreases by 4%, while the CuCe_x-SSZ-16-750HT series catalysts have little change compared with CuCe_x-SSZ-16-Fresh. The selectivity of NO₂ byproducts is below 2% for CuCe_x-SSZ-16-750HT series catalysts in the whole temperature range. As for N₂O, the selectivity for Cu-SSZ-16-750HT is 6% at 150 °C, compared to 4% for the CuCe_x-SSZ-16-750HT series catalysts.

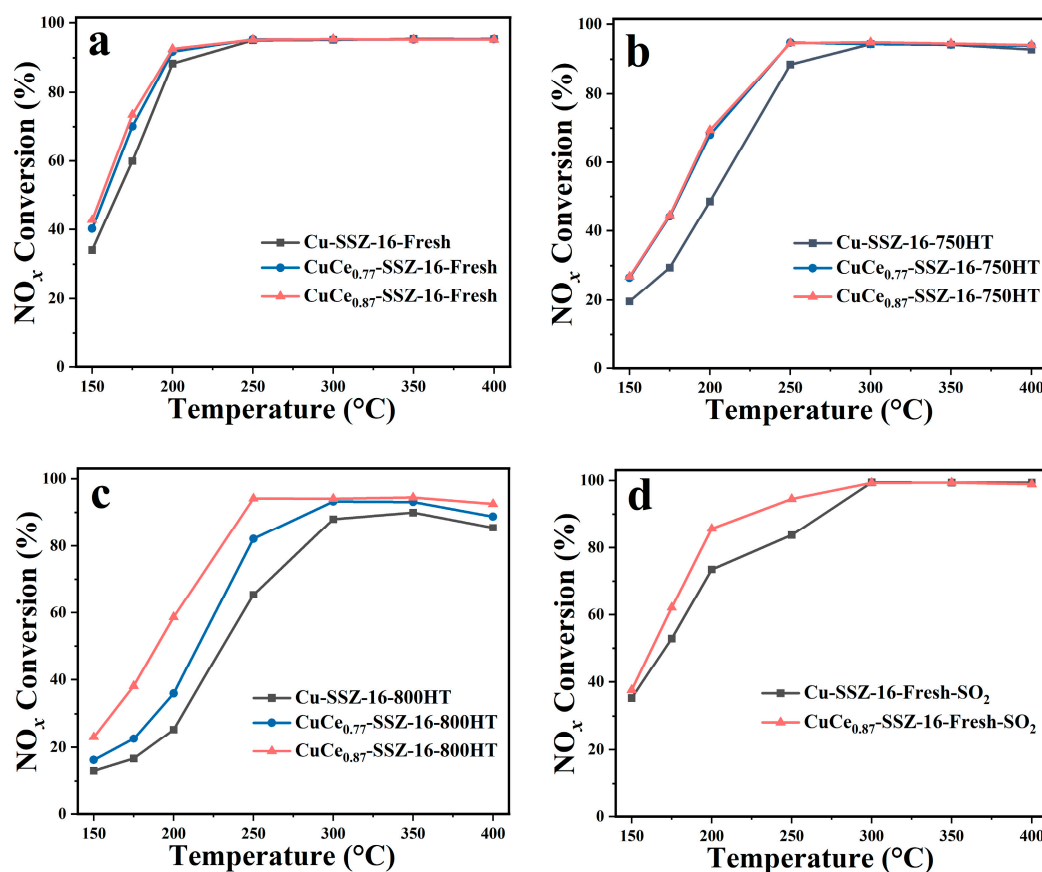


Figure 1. NO_x conversion before (a), after hydrothermal treatments at 750 °C (b) and 800 °C (c), and in the presence of SO₂ (d) over Cu-SSZ-16, CuCe_{0.77}-SSZ-16, and CuCe_{0.87}-SSZ-16. Reaction conditions: 500 ppm NO, 500 ppm NH₃, 50 ppm SO₂ (when used), 5 vol% O₂, 5 vol% H₂O, balance N₂, and GHSV = 200,000 h⁻¹.

Additionally, to further investigate the effect of incorporating Ce on the hydrothermal stability of CuCe_x-SSZ-16, the catalysts were hydrothermally aged under more severe conditions of 800 °C. As shown in Figure 1c, the NO_x conversion of Cu-SSZ-16-800HT is below 90% at 150–400 °C. After introducing Ce species, the NO_x reduction efficiency of CuCe_{0.77}-SSZ-16-800HT and CuCe_{0.87}-SSZ-16-800HT is above 90% at 285–400 °C and 245–400 °C, respectively. The corresponding N₂ selectivity of the CuCe_x-SSZ-16-800HT series catalysts shows a noticeable improvement below 250 °C (Figure S1g). The N₂ selectivity of Cu-SSZ-16-800HT is only 85% at 150 °C, while that of the CuCe_{0.77}-SSZ-16-800HT and CuCe_{0.87}-SSZ-16-800HT catalysts is 89% and 93% at the same temperature, respectively. The three samples aged at 800 °C maintain similar low NO₂ selectivity (Figure S1h). Compared with Cu-SSZ-16-800HT, the N₂O selectivity of CuCe_{0.77}-SSZ-16-800HT and CuCe_{0.87}-SSZ-16-800HT significantly declines at low temperatures, decreasing from 10% to 7% and then to 4% at 150 °C (Figure S1i). It is suggested that the addition of Ce improves the hydrothermal stability of the catalysts and enables the aged catalysts to maintain better NH₃-SCR performance.

The CuCe_{0.87}-SSZ-16-Fresh catalyst was selected to explore the influence of SO₂ in the reaction mixture, and the experimental results are depicted in Figure 1d. In the presence of SO₂, the NH₃-SCR performance of CuCe_{0.87}-SSZ-16-Fresh-SO₂ (where “SO₂” represents 50 ppm SO₂ in the feed gas) is well maintained at the low-temperature range (<300 °C). The catalytic activity of Cu-SSZ-16 significantly decreases due to the toxicity of SO₂, compared with Cu-SSZ-16-Fresh, the NO_x conversion decreases by 11% at 250 °C for Cu-SSZ-16-Fresh-SO₂. Meanwhile, CuCe_{0.87}-SSZ-16-Fresh-SO₂ shows 94% NO_x conversion at 250 °C, which

is virtually identical to that of CuCe_{0.87}-SSZ-16-Fresh, suggesting that the introduction of Ce improves the SO₂ resistance of the catalysts.

According to the above results, it can be inferred that the incorporation of Ce positively impacts the low-temperature NH₃-SCR performance and the SO₂ resistance. More importantly, it improves the hydrothermal stability of the CuCe_x-SSZ-16 series catalysts. Moreover, with the increase in the Ce contents, the positive effect is enhanced, and CuCe_{0.87}-SSZ-16 exhibits the best hydrothermal stability.

2.2. Structural Characterization

The chemical compositions of the fresh and aged catalysts are exhibited in Table 1. The fresh catalysts contain similar Si/Al ratios and Cu contents. In addition, the changes in Cu and Ce contents after hydrothermal treatment at 800 °C may be due to the destruction of the framework [29]. Figure 2a,b, shows the PXRD patterns of the fresh catalysts and the samples aged at 800 °C. As presented in Figure 2a, the PXRD patterns of the fresh catalysts exhibit the typical characteristic peaks of SSZ-16 ($2\theta = 7.4^\circ, 8.6^\circ, 11.6^\circ, \text{ and } 12.8^\circ$), implying that the AFX structure is well maintained after Cu and Ce ion exchange [31]. After hydrothermally aging at 800 °C, an amorphous structure forms in the three aged catalysts, possibly due to structural damage caused by hydrothermal treatments. Among them, the characteristic peaks of the AFX structure can be identified in the PXRD pattern of CuCe_{0.87}-SSZ-16-800HT. It is suggested that CuCe_{0.87}-SSZ-16-800HT maintains a partial AFX structure, which is important for CuCe_{0.87}-SSZ-16-800HT to exhibit high deNO_x activity still. However, the characteristic peaks of SSZ-16 could barely be recognized for Cu-SSZ-16-800HT, indicating that the structure has collapsed after hydrothermal treatment at 800 °C. Notably, although the crystallinity decreases significantly, no characteristic peaks corresponding to CuO_x and CeO₂ are found on all the fresh and aged catalyst samples [32,33], indicating that CuO_x or CeO₂ particles have not formed and the Cu and Ce are distributed well in all catalysts.

Table 1. The chemical compositions and textural parameters of Cu-SSZ-16-Fresh, CuCe_{0.77}-SSZ-16-Fresh, CuCe_{0.87}-SSZ-16-Fresh, Cu-SSZ-16-800HT, CuCe_{0.77}-SSZ-16-800HT, and CuCe_{0.87}-SSZ-16-800HT.

Catalysts	Component Content ^a			S _{BET} ^b (m ² ·g ⁻¹)	Pore Volume ^b (cm ³ ·g ⁻¹)
	Si/Al	Cu (wt.%)	Ce (wt.%)		
Cu-SSZ-16-Fresh	3.4	2.2	-	523	0.247
CuCe _{0.77} -SSZ-16-Fresh	3.4	2.2	0.77	577	0.251
CuCe _{0.87} -SSZ-16-Fresh	3.3	2.1	0.87	605	0.261
Cu-SSZ-16-800HT	3.1	2.8	-	13	0.030
CuCe _{0.77} -SSZ-16-800HT	3.1	2.8	1.0	30	0.035
CuCe _{0.87} -SSZ-16-800HT	3.1	2.7	1.1	37	0.060

^a Measured by ICP-OES. ^b Derived from N₂ adsorption–desorption isotherms.

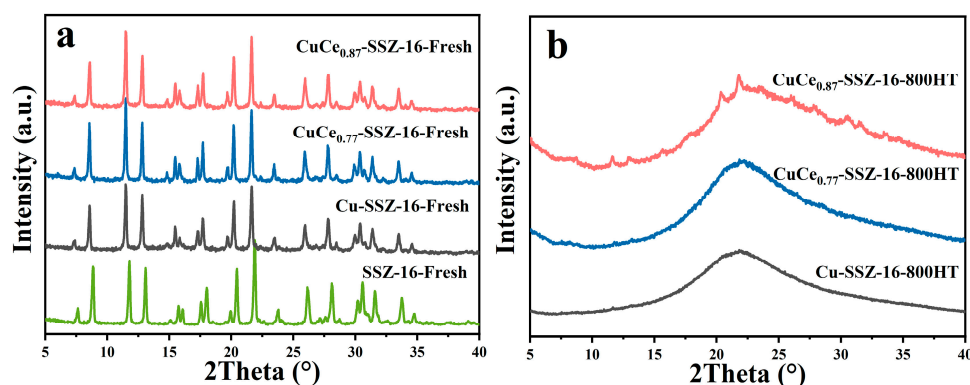


Figure 2. PXRD patterns before (a) and after hydrothermal treatment at 800 °C (b) of SSZ-16, Cu-SSZ-16, CuCe_{0.77}-SSZ-16, and CuCe_{0.87}-SSZ-16.

The N_2 adsorption–desorption analyses for Cu-SSZ-16-Fresh, $CuCe_{0.77}$ -SSZ-16-Fresh, and $CuCe_{0.87}$ -SSZ-16-Fresh are demonstrated in Figure 3a,b. All three fresh catalysts show type I isotherms related to typical microporous structures. Table 1 summarizes the BET surface areas (S_{BET}) and pore volumes of the fresh and aged catalysts. The table shows that the S_{BET} values are 523, 577, and 605 $m^2 \cdot g^{-1}$ for Cu-SSZ-16-Fresh, $CuCe_{0.77}$ -SSZ-16-Fresh, and $CuCe_{0.87}$ -SSZ-16-Fresh, respectively. Correspondingly, the pore volumes gradually increase from 0.247 $cm^3 \cdot g^{-1}$ to 0.251 $cm^3 \cdot g^{-1}$, then to 0.261 $cm^3 \cdot g^{-1}$. In general, both S_{BET} and pore volumes increase with an increase in the Ce mass fraction, and $CuCe_{0.87}$ -SSZ-16-Fresh has the largest S_{BET} and pore volumes. However, the S_{BET} and pore volumes decline sharply after hydrothermal treatment at 800 °C, which may be due to the collapse of the zeolite skeleton. The S_{BET} and pore volumes of Cu-SSZ-16-800HT are only 13 $m^2 \cdot g^{-1}$ and 0.030 $cm^3 \cdot g^{-1}$, respectively, while they are 30 $m^2 \cdot g^{-1}$ and 0.035 $cm^3 \cdot g^{-1}$ for $CuCe_{0.77}$ -SSZ-16-800HT and 37 $m^2 \cdot g^{-1}$ and 0.060 $cm^3 \cdot g^{-1}$ for $CuCe_{0.87}$ -SSZ-16-800HT. The skeleton of Cu-SSZ-16-800HT collapses more severely, which is consistent with the PXRD results. Pore structures are retained in the aged catalysts, which may help the catalysts maintain catalytic activity.

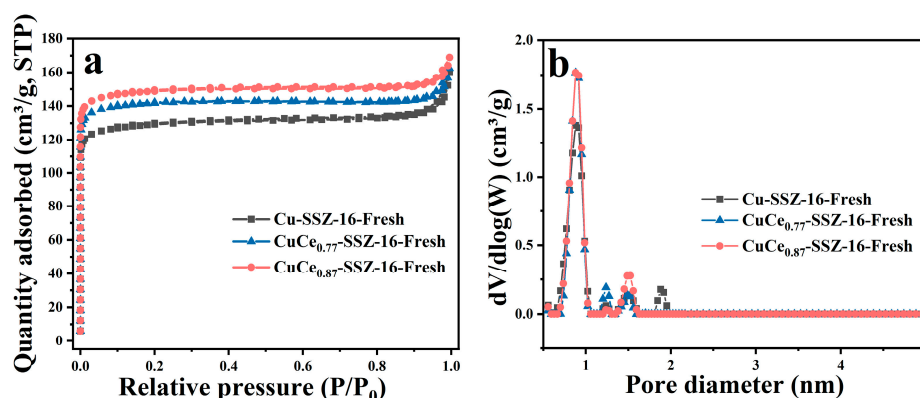


Figure 3. (a) N_2 adsorption–desorption isotherms and (b) Pore-size distribution spectra of Cu-SSZ-16-Fresh, $CuCe_{0.77}$ -SSZ-16-Fresh, and $CuCe_{0.87}$ -SSZ-16-Fresh.

Figure 4 displays the SEM results of the fresh catalysts at different magnifications. All the samples show similar morphologies of a double-cone prism with a similar average length of 1–2 μm . It can be concluded that the incorporation of Ce does not affect the structure or morphology of the catalysts. However, the morphology changed after hydrothermal treatment at 800 °C due to the damage to the zeolite framework (Figure S2). As shown in Figure 5, the TEM in bright and dark fields and corresponding element mapping images illustrate that both the Cu and Ce atoms are well dispersed in the catalyst samples, in agreement with the PXRD results mentioned above. Moreover, CuO_x or CeO_x clusters are not detected, leading to improved NH_3 -SCR performance.

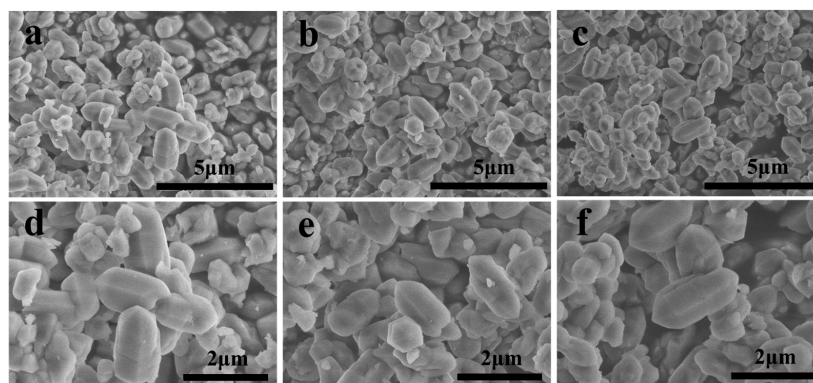


Figure 4. SEM images of Cu-SSZ-16-Fresh (a,d), $CuCe_{0.77}$ -SSZ-16-Fresh (b,e), and $CuCe_{0.87}$ -SSZ-16-Fresh (c,f).

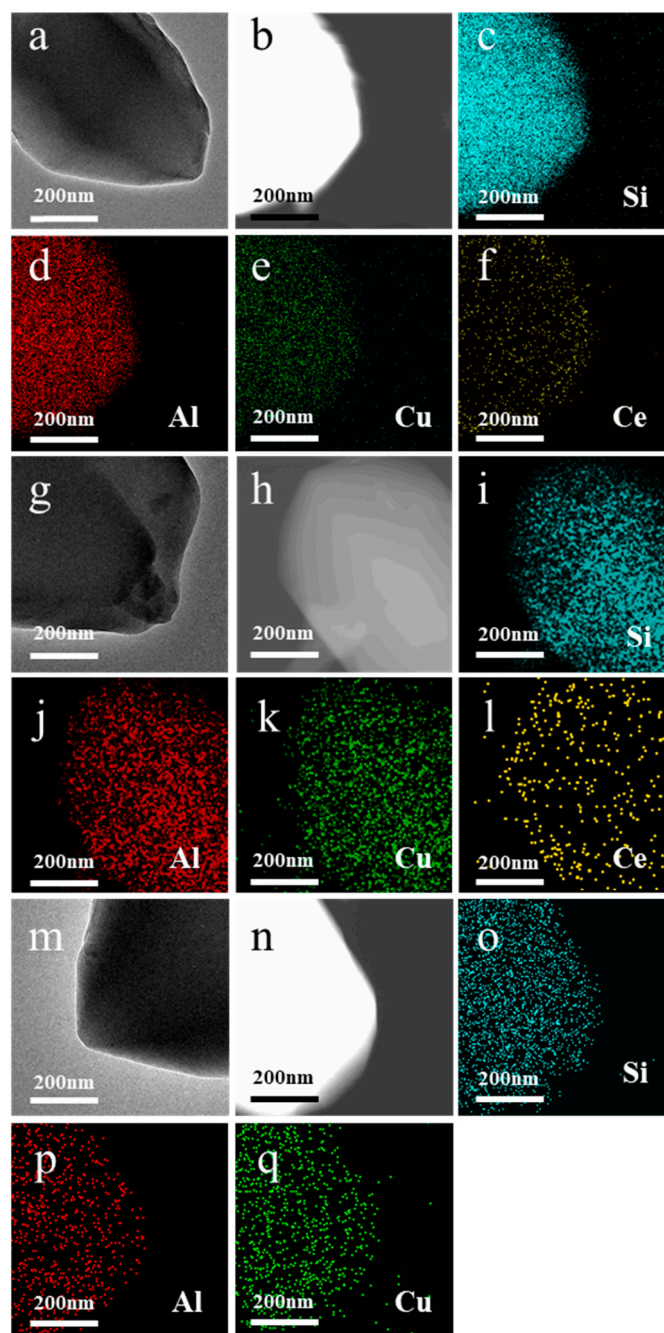


Figure 5. TEM in bright and dark fields and EDS mapping images of $\text{CuCe}_{0.87}\text{-SSZ-16-Fresh}$ (a–f), $\text{CuCe}_{0.77}\text{-SSZ-16-Fresh}$ (g–l), and Cu-SSZ-16-Fresh (m–q).

The ^{27}Al MAS NMR spectra of SSZ-16-Fresh, Cu-SSZ-16-Fresh , $\text{CuCe}_{0.77}\text{-SSZ-16-Fresh}$, and $\text{CuCe}_{0.87}\text{-SSZ-16-Fresh}$ are depicted in Figure 6a. Four peaks are determined at around 57, 51, 30, and -1 ppm in the spectra of Cu-SSZ-16-Fresh , $\text{CuCe}_{0.77}\text{-SSZ-16-Fresh}$, and $\text{CuCe}_{0.87}\text{-SSZ-16-Fresh}$, respectively. For SSZ-16-Fresh, there are only three peaks, leaving out the peak at 30 ppm. The 57 ppm and 51 ppm signals are associated with two kinds of framework aluminum in zeolite; the former is attributed to tetrahedrally coordinated aluminum, and the latter corresponds to distorted aluminum [22,34]. The peak signals centered at 30 ppm and -1 ppm are characteristic of penta-coordinated and octahedral aluminum, respectively [35]. The peaks are integrally calculated and represented in Figure S3 and Table 2. The percentage of octahedral aluminum in SSZ-16-Fresh is 0.9%, which increases to 11.8% for Cu-SSZ-16-Fresh . It may be due to the distortion of the zeolite

skeleton caused by Cu ion exchange, leading to the dealumination of the catalyst [34]. After Ce ion exchange, the relative content of octahedral aluminum decreases from 11.8% to 9.7% and 6.8%. The amount of tetrahedrally coordinated aluminum is markedly enhanced from 19.9% to 25.1% and 27.2%, indicating that the incorporation of Ce increases the framework Al over CuCe_x-SSZ-16-Fresh. The proportions of framework Al increase with an increase in Ce. After hydrothermal treatment at 800 °C, the peaks at 52 ppm and 0 ppm occupy a dominant position for Cu-SSZ-16-800HT (Figure 6b). Compared with the Cu-SSZ-16-Fresh, the non-framework Al accounts for a larger proportion of aluminum in the Cu-SSZ-16-800HT. Furthermore, the framework Al in Cu-SSZ-16-800HT is mainly composed of distorted aluminum. However, the peak at 57 ppm remains in the ²⁷Al MAS NMR spectra of CuCe_x-SSZ-16-800HT, demonstrating that more tetrahedrally coordinated aluminum exists in the CuCe_x-SSZ-16-800HT series catalysts [5]. Compared with CuCe_x-SSZ-16-Fresh, although the non-framework Al increases in CuCe_x-SSZ-16-800HT, the framework Al still accounts for the majority of aluminum in CuCe_x-SSZ-16-800HT. It may be one of the reasons why the CuCe_x-SSZ-16-800HT series catalysts can still maintain high NH₃-SCR catalytic activity. It is concluded that introducing Ce into the Cu-SSZ-16 catalysts reduces the dealumination reaction and improves the crystallinity, leading to outstanding hydrothermal stability.

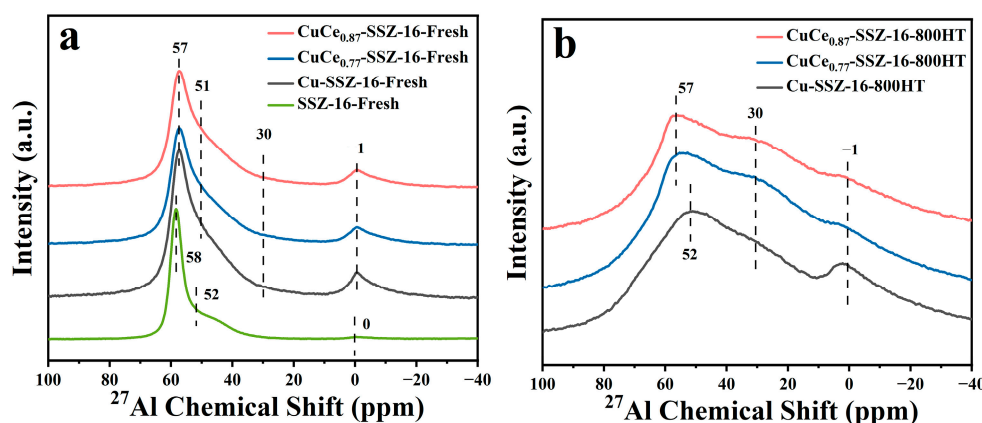


Figure 6. ²⁷Al MAS NMR spectra of (a) SSZ-16-Fresh, Cu-SSZ-16-Fresh, CuCe_{0.77}-SSZ-16-Fresh and CuCe_{0.87}-SSZ-16-Fresh, and (b) Cu-SSZ-16-800HT, CuCe_{0.77}-SSZ-16-800HT, and CuCe_{0.87}-SSZ-16-800HT.

Table 2. Quantitative analysis of the ²⁷Al NMR results of SSZ-16-Fresh, Cu-SSZ-16-Fresh, CuCe_{0.77}-SSZ-16-Fresh, and CuCe_{0.87}-SSZ-16-Fresh.

Catalysts	²⁷ Al NMR Peak/ppm Relative Concentration (%)			
	57	51	30	−1
SSZ-16-Fresh	45.8	53.3	-	0.9
Cu-SSZ-16-Fresh	19.9	61.5	6.8	11.8
CuCe _{0.77} -SSZ-16-Fresh	25.1	58.1	7.1	9.7
CuCe _{0.87} -SSZ-16-Fresh	27.2	56.9	9.1	6.8

Furthermore, to investigate the change in the surface acidity, NH₃-TPD measurements were carried out on Cu-SSZ-16-Fresh, CuCe_{0.77}-SSZ-16-Fresh, and CuCe_{0.87}-SSZ-16-Fresh (Figure 7a). All the catalysts exhibit three desorption peaks at around 197, 318, and 505 °C (referred to as S1, S2, and S3, respectively). The signal at 197 °C is related to the weak acid sites, including physically adsorbed NH₃, NH₃ adsorbed on weak Brønsted acid sites, and NH₃ adsorbed by the surface hydroxyl groups [22,27,36]. The 318 °C peak is associated with moderate Lewis acid sites produced by ion exchange [30]. The peak at 505 °C is attributed to the NH₃ adsorbed on strong Brønsted acid sites [27]. It can be found that all the samples display similar locations and amounts of acid sites. The deconvolution areas of the fresh catalysts are shown in Figure 7b. With the incorporation of Ce, the amount of the weak acid sites (S1) decreases slightly, which may be due to the introduced Ce occupying some

Brønsted acid sites [37]. The number of moderate and strong acid sites (S2 and S3) increases with the addition of Ce, which is beneficial for NH₃ storage and NH₃-SCR performance.

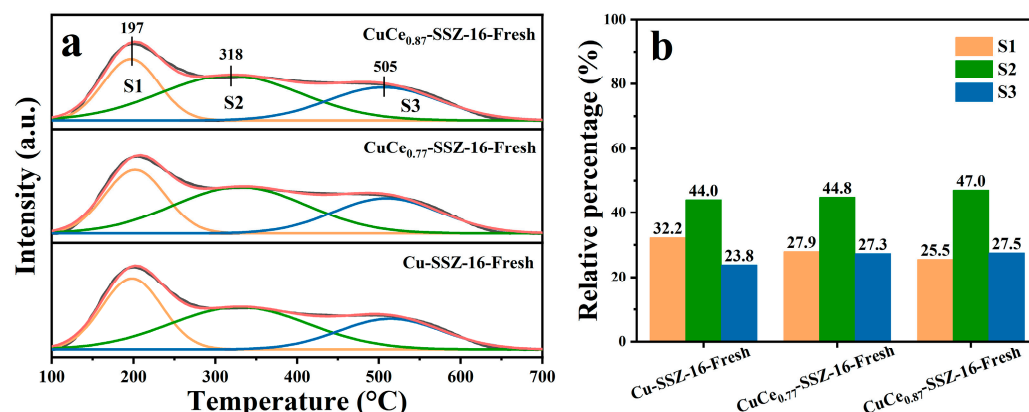


Figure 7. (a) Deconvolution of the NH₃-TPD curves and (b) the corresponding areas over Cu-SSZ-16-Fresh, CuCe_{0.77}-SSZ-16-Fresh, and CuCe_{0.87}-SSZ-16-Fresh.

2.3. Cu and Ce Species

XPS was performed to inquire about the chemical state of the two species introduced, and the XPS results of the fresh samples are exhibited in Figure 8. The Cu 2p spectrum (Figure 8a) is divided into two peaks at around 933.1 and 935.9 eV, which may correspond to the presence of Cu⁺ and Cu²⁺ species [28,33,38,39]. The integral area fraction results of Cu-SSZ-16-Fresh, CuCe_{0.77}-SSZ-16-Fresh, and CuCe_{0.87}-SSZ-16-Fresh are depicted in Table 3. The relative amount of Cu²⁺ significantly increases from 32.8% to 40.4% and then to 62.6%, while the proportion of Cu⁺ decreases as Ce increases, revealing that the addition of Ce facilitates the formation of surface Cu²⁺. Moreover, the Ce 3d spectra of CuCe_{0.77}-SSZ-16-Fresh and CuCe_{0.87}-SSZ-16-Fresh are obtained (Figure 8b). According to the literature, the spectra can be recognized as having eight peaks, and the ones marked u' and v' are related to Ce³⁺ species; the others, which are labeled u, v, u'', v'', u''' and v''', are ascribed to Ce⁴⁺ species [40–43]. As generalized in Table 3, the Ce³⁺/(Ce³⁺ + Ce⁴⁺) ratios increase from 44.4% to 54.4% over the surface with an increase in the Ce contents, which is due to the formation of Cu²⁺ in the redox cycles Cu⁺ + Ce⁴⁺ → Cu²⁺ + Ce³⁺ [37,44]. Consequently, the addition of Ce leads to the electron transfer of Cu⁺, forming more Cu²⁺ and contributing to the high NH₃-SCR activity. The XPS results of the catalysts aged at 800 °C are displayed in Figure S4, and the deconvolution areas are listed in Table 3. After hydrothermal treatment at 800 °C, the percentage of Cu²⁺ decreases from 32.8% to 20.7% in Cu-SSZ-16 because hydrothermal aging transfers some of the Cu²⁺ to CuO_x [45]. The proportion of Cu²⁺ in CuCe_{0.77}-SSZ-16-800HT and CuCe_{0.87}-SSZ-16-800HT is 33.5% and 35.8%, respectively. Although the proportion decreases compared with CuCe_{0.77}-SSZ-16-Fresh and CuCe_{0.87}-SSZ-16-Fresh, it is still higher than that of Cu-SSZ-16-Fresh (32.8%). Many active Cu²⁺ species are retained in the CuCe_x-SSZ-16-800HT samples, which is an important reason for the low deactivation of CuCe_x-SSZ-16-800HT series catalysts. The ratio of Ce³⁺/(Ce³⁺ + Ce⁴⁺) declines, meaning that the redox ability of the aged catalysts is reduced by the hydrothermal treatment [46]. Even though the relative amounts of Cu²⁺ and Ce³⁺ decrease for CuCe_x-SSZ-16-800HT, many remain in the aged catalysts, inhibiting a sharp decline in catalytic activity. It is suggested that the introduction of Ce could increase the active Cu²⁺ contents and improve the resistance to hydrothermal treatments [28].

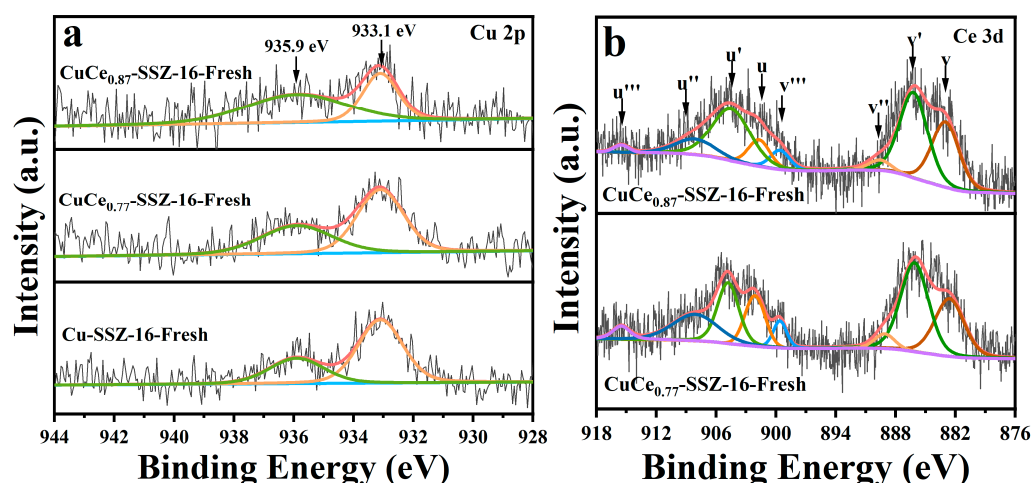


Figure 8. XPS spectra of Cu 2p (a) and Ce 3d (b) for Cu-SSZ-16-Fresh, CuCe_{0.77}-SSZ-16-Fresh, and CuCe_{0.87}-SSZ-16-Fresh.

Table 3. The distribution of Cu and Ce species revealed by XPS.

Catalysts	Cu ²⁺ (%)	Cu ⁺ (%)	Ce ³⁺ /(Ce ³⁺ + Ce ⁴⁺) (%)
Cu-SSZ-16-Fresh	32.8	67.2	-
CuCe _{0.77} -SSZ-16-Fresh	40.4	59.6	44.4
CuCe _{0.87} -SSZ-16-Fresh	62.6	37.4	54.4
Cu-SSZ-16-800HT	20.7	79.3	-
CuCe _{0.77} -SSZ-16-800HT	33.5	66.5	37.8
CuCe _{0.87} -SSZ-16-800HT	35.8	64.2	43.0

Figure S5 shows the UV-vis spectra of the fresh catalysts. All three catalysts display two peaks at 202 and 733 nm, related to the charge transfer from the framework oxygen to Cu²⁺ and the d-d transitions of Cu²⁺ in CuO_x [12,47]. However, due to the good distribution and relatively low content of CuO_x, the peaks related to CuO_x cannot be detected by PXRD. Additionally, a new peak appears at 297 nm for CuCe_{0.77}-SSZ-16-Fresh and CuCe_{0.87}-SSZ-16-Fresh, assigned to the charge transfer process of Ce³⁺ [48]. The intensity of the 202 nm peak for CuCe_{0.77}-SSZ-16-Fresh and CuCe_{0.87}-SSZ-16-Fresh is significantly higher than that of Cu-SSZ-16-Fresh, implying that more Cu²⁺ species exist in CuCe_{0.77}-SSZ-16-Fresh and CuCe_{0.87}-SSZ-16-Fresh. Hence, it can be inferred that adding Ce contributes to the rise in Cu²⁺ species in the catalysts, and the more pronounced effect is enhanced with an increase in the Ce contents. The peak located at 297 nm suggests the existence of Ce³⁺ in the CuCe_x-SSZ-16-Fresh series catalysts. Therefore, the incorporation of Ce might contribute to the formation of Cu²⁺, which is also proven by the XPS results.

EPR was measured to evaluate the quantity and coordination environment of the Cu²⁺ species in zeolites because Cu⁺ and CuO_x species could not be detected by EPR [49]. Figure S6 depicts the EPR results of Cu-SSZ-16-Fresh, CuCe_{0.77}-SSZ-16-Fresh, and CuCe_{0.87}-SSZ-16-Fresh. The three samples show similar peak features. The sharp peaks ($g_{\perp} = 2.08$) can be observed in all the samples, which correspond to isolated Cu²⁺ coordinated with oxygen. After the introduction of Ce, the intensities of the $g_{\perp} = 2.08$ peaks are significantly enhanced. The enhancement is greater with an increase in the Ce content, suggesting that the quantity of Cu²⁺ gradually increases with the addition of Ce. Furthermore, the hyperfine features of EPR are $g_{\parallel} = 2.37$ for Cu-SSZ-16-Fresh and CuCe_{0.77}-SSZ-16-Fresh, demonstrating that the Cu²⁺ species are in the identical coordination environment in the two samples. For CuCe_{0.87}-SSZ-16-Fresh, the hyperfine feature has $g_{\parallel} = 2.33$ due to the different coordination environments of Cu²⁺ after the incorporation of Ce.

Additionally, to explore the distribution and amount of Cu species in the catalysts, H₂-TPR was measured over the fresh catalysts (Figure 9a) and the samples aged at 800 °C (Figure 9b). The H₂-TPR spectrum of Cu-SSZ-16-Fresh is deconvoluted into five reduction

peaks at approximately 236 °C, 323 °C, 390 °C, 477 °C, and 519 °C, with each peak representing one kind of Cu species. Among these, the 236 °C peak corresponds to $[\text{Cu}(\text{OH})]^+-\text{Z}$, while that at 390 °C is related to $\text{Cu}^{2+}-2\text{Z}$. Notably, $\text{Cu}^{2+}-2\text{Z}$ species require a higher temperature to be reduced since they are situated in the 6-ring and are more stable. The peak at 323 °C is associated with CuO_x , which exerts negative effects on NH_3 -SCR performance by blocking the pores of the zeolite catalysts. The signal at 477 °C is assigned to $\text{Cu}(\text{AlO}_2)_2$ in the catalysts, which is indirectly caused by the dealumination of the zeolite framework. Cu^+ species in the catalysts are reduced to Cu^0 at 519 °C [50–52]. Furthermore, the H_2 -TPR curves of $\text{CuCe}_{0.77}\text{-SSZ-16-Fresh}$ and $\text{CuCe}_{0.87}\text{-SSZ-16-Fresh}$ show five deconvolution regions similar to those of Cu-SSZ-16-Fresh . Table 4 lists the integral calculation of the H_2 -TPR profiles in the range of 100–400 °C. As presented here, the CuO_x species account for 26.2% of the Cu-SSZ-16-Fresh catalyst but 19.4% and 11.5% of the $\text{CuCe}_{0.77}\text{-SSZ-16-Fresh}$ and $\text{CuCe}_{0.87}\text{-SSZ-16-Fresh}$ catalysts, indicating that the modification of Ce combats the generation of CuO_x . The percentage of $[\text{Cu}(\text{OH})]^+-\text{Z}$ is 11.8%, while that of $\text{Cu}^{2+}-2\text{Z}$ is 62.0% in Cu-SSZ-16-Fresh . After adding Ce, the proportions of $[\text{Cu}(\text{OH})]^+-\text{Z}$ and $\text{Cu}^{2+}-2\text{Z}$ increase to 13.0% and 67.6% in the $\text{CuCe}_{0.77}\text{-SSZ-16-Fresh}$ catalyst, respectively. Moreover, $[\text{Cu}(\text{OH})]^+-\text{Z}$ accounts for 14.1%, and $\text{Cu}^{2+}-2\text{Z}$ accounts for 74.4% in the $\text{CuCe}_{0.87}\text{-SSZ-16-Fresh}$ catalyst when the Ce contents increase further. The two Cu^{2+} species increase with an increase in Ce. Different from the fresh catalysts, the curves are only determined to have four peaks after hydrothermal treatment at 800 °C, namely, at 339 °C, 421 °C, 560 °C, and 698 °C, related to CuO_x , $\text{Cu}^{2+}-2\text{Z}$, $\text{Cu}(\text{AlO}_2)_2$, and Cu^+ , respectively [52]. The peaks shift toward high temperatures, which suggests that these Cu species have become more stable during the hydrothermal treatment at 800 °C [52,53]. It is observed that the peak at about 230 °C disappears after hydrothermal aging because the $[\text{Cu}(\text{OH})]^+-\text{Z}$ is unstable and transforms to $\text{Cu}^{2+}-2\text{Z}$ or CuO_x species at high temperatures [21]. This can also explain why the low-temperature catalytic activity of the aged samples significantly decreases. As presented in Table 4, compared with the fresh samples, the proportion of CuO_x increases and the proportion of $\text{Cu}^{2+}-2\text{Z}$ declines in the samples aged at 800 °C. However, most $\text{Cu}^{2+}-2\text{Z}$ species are retained in the aged catalysts, preventing a significant decrease in NH_3 -SCR performance. The percentages of $\text{Cu}^{2+}-2\text{Z}$ species in Cu-SSZ-16-800HT , $\text{CuCe}_{0.77}\text{-SSZ-16-800HT}$, and $\text{CuCe}_{0.87}\text{-SSZ-16-800HT}$ are 51.4%, 54.0%, and 56.0%, respectively. Compared with Cu-SSZ-16-800HT , more active $\text{Cu}^{2+}-2\text{Z}$ species are maintained in $\text{CuCe}_x\text{-SSZ-16-800HT}$, which helps the $\text{CuCe}_x\text{-SSZ-16-800HT}$ catalysts maintain high deNO_x catalytic activity. The proportion of CuO_x is 48.6%, compared to 46.0% and 44.0% for $\text{CuCe}_{0.77}\text{-SSZ-16-800HT}$ and $\text{CuCe}_{0.87}\text{-SSZ-16-800HT}$, respectively, confirming that the introduction of Ce can effectively prevent the formation of CuO_x . Therefore, it can be deduced that the formation of Cu^{2+} is promoted while the generation of CuO_x is inhibited by introducing Ce, leading to higher hydrothermal stability.

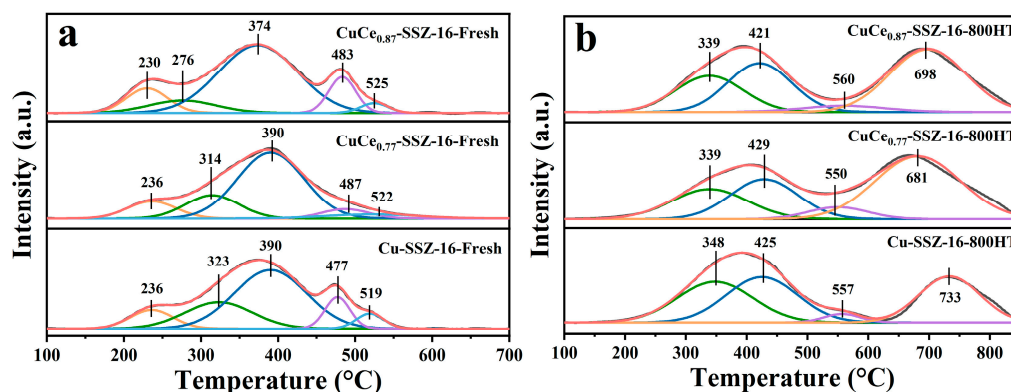
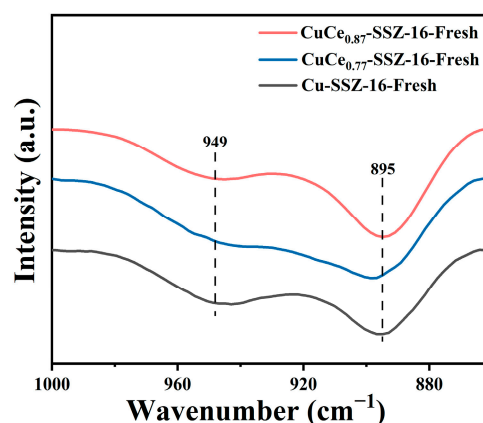


Figure 9. H_2 -TPR before (a) and after hydrothermal treatment at 800 °C (b) of Cu-SSZ-16 , $\text{CuCe}_{0.77}\text{-SSZ-16}$, and $\text{CuCe}_{0.87}\text{-SSZ-16}$.

Table 4. The distribution of Cu species measured by H₂-TPR.

Catalysts	[Cu(OH)] ⁺ -Z (%)	Cu ²⁺ -2Z (%)	CuO _x (%)
Cu-SSZ-16-Fresh	11.8	62.0	26.2
CuCe _{0.77} -SSZ-16-Fresh	13.0	67.6	19.4
CuCe _{0.87} -SSZ-16-Fresh	14.1	74.4	11.5
Cu-SSZ-16-800HT	-	51.4	48.6
CuCe _{0.77} -SSZ-16-800HT	-	54.0	46.0
CuCe _{0.87} -SSZ-16-800HT	-	56.0	44.0

In situ DRIFTS measurements under NH₃ adsorption are ideal for probing the relative contributions of the two Cu²⁺ species in the catalysts. The NH₃-DRIFTS results of Cu-SSZ-16-Fresh, CuCe_{0.77}-SSZ-16-Fresh, and CuCe_{0.87}-SSZ-16-Fresh are displayed in Figure 10. Two negative peaks appear in 860–1000 cm⁻¹ wave numbers, one corresponding to [Cu(OH)]⁺-Z at 949 cm⁻¹ and the other related to Cu²⁺-2Z at 895 cm⁻¹ [13,54,55]. The two peak intensities increase effectively, demonstrating that the amounts of the two Cu²⁺ species increase through the introduction of Ce. The relative integral areas are shown in Figure S7, revealing that the relative content of the two Cu²⁺ species also changes with the addition of Ce. The percentage of Cu²⁺-2Z in Cu-SSZ-16-Fresh is 48.7%, which increases to 51.5% and 54.3% for CuCe_{0.77}-SSZ-16-Fresh and CuCe_{0.87}-SSZ-16-Fresh, respectively. With an increase in the Ce contents, the relative proportion of Cu²⁺-2Z increases gradually, and the percentage of [Cu(OH)]⁺-Z decreases. It is indicated that Ce addition is conducive to forming Cu²⁺ species, especially Cu²⁺-2Z species, which is beneficial to the hydrothermal stability of the catalysts.

**Figure 10.** In situ DRIFTS spectra of Cu-SSZ-16-Fresh, CuCe_{0.77}-SSZ-16-Fresh, and CuCe_{0.87}-SSZ-16-Fresh.

From the analysis results above, we can conclude that the incorporation of Ce can stabilize the skeleton of Cu-SSZ-16 and also promote the formation of [Cu(OH)]⁺-Z and Cu²⁺-2Z, especially Cu²⁺-2Z. The PXRD results show that the AFX structure is retained in the hydrothermally treated CuCe_x-SSZ-16, suggesting that adding Ce can improve the structural stability of the catalysts. The ²⁷Al MAS NMR results also confirm this deduction, as the dealumination is reduced and the framework Al increases in fresh and aged catalysts with Ce. Additionally, the framework Al is better maintained in CuCe_x-SSZ-16-800HT, contributing to the excellent NH₃-SCR performance of CuCe_x-SSZ-16-800HT. To further investigate the promotional effect of introducing Ce, XPS, EPR, UV-vis, H₂-TPR, and in situ DRIFTS analyses were conducted. The XPS results show that the percentage of Cu²⁺ species is only 32.8% for Cu-SSZ-16-Fresh but rises to 40.4% and 62.6% for CuCe_{0.77}-SSZ-16-Fresh and CuCe_{0.87}-SSZ-16-Fresh, respectively, after the introduction of Ce. Correspondingly, the Ce and Cu species constitute a redox cycle: Cu⁺ + Ce⁴⁺ → Cu²⁺ + Ce³⁺, meaning that the incorporation of Ce is able to increase the Cu²⁺ species in catalysts. After hydrothermal treatment at 800 °C, although the amount of Cu²⁺ species decreases for CuCe_{0.77}-SSZ-16-

800HT and CuCe_{0.87}-SSZ-16-800HT, it is still higher than that of Cu-SSZ-16-Fresh. The majority of Cu²⁺ is still retained in the CuCe_x-SSZ-16-800HT series catalysts, accounting for high NH₃-SCR activity. The EPR and UV-vis measurements exhibit similar results to those of XPS, namely that the amounts of Cu²⁺ increase obviously with the addition of Ce. For the H₂-TPR analysis, the results suggest that the relative amount of CuO_x reduces from 26.2% to 19.4% and then to 11.5% for the fresh samples. Meanwhile, the proportion of active Cu²⁺ rises after the incorporation of Ce. After hydrothermal aging at 800 °C, even though Cu²⁺-2Z decreases in the aged catalysts, most active Cu²⁺-2Z species are retained in the aged catalysts, which is an important reason for the low deactivation of CuCe_x-SSZ-16-800HT series catalysts. It is confirmed that the incorporation of Ce can promote the formation of active Cu²⁺ but limit the increase in CuO_x. Moreover, the in situ DRIFTS results reveal that adding Ce would significantly increase the relative content of Cu²⁺-2Z, contributing to remarkable hydrothermal stability. In summary, the introduction of Ce can improve the stability of the Cu-exchanged zeolite skeleton and increase the active Cu²⁺ species in catalysts, thus improving hydrothermal stability. Furthermore, the zeolite skeleton structure and active Cu²⁺ species are better maintained in the samples hydrothermally aged at 800 °C, leading to low deactivation of the CuCe_x-SSZ-16-800HT series catalysts.

3. Materials and Methods

3.1. Synthesis and Hydrothermal Treatments

Based on a previous report, the SSZ-16 catalyst was synthesized with a composition of SiO₂: 0.045 Al₂O₃: 0.11 OSDA: 0.8 NaOH: 20 H₂O at 150 °C for 9 days [10]. The detailed procedures are available in the Electronic Supplementary Information (ESI). The Cu-SSZ-16 catalyst was obtained by successively exchanging the prepared SSZ-16 with a 0.1 M CH₃COONH₄ and a 0.01 M Cu(NO₃)₂ solution. Then, Cu-SSZ-16 was exchanged with a Ce(NO₃)₃ solution of different concentrations at 80 °C overnight to obtain the CuCe_x-SSZ-16 series catalysts. After drying at 100 °C, the catalyst products were calcined in air at 290 °C for 2 h and then at 550 °C for 6 h, thus producing the fresh catalysts. Then the fresh samples were hydrothermally aged at different temperatures in air containing 10 vol% H₂O for 10 h to obtain the aged samples.

3.2. Characterization of the Catalysts

The powder X-ray diffraction (PXRD) was applied to analyze the zeolite products with a Bruker D2 Phaser instrument at a scanning speed of 0.2° s⁻¹. The N₂ adsorption-desorption analyses were performed on a Micrometrics ASAP 2020 Plus apparatus at the temperature of liquid nitrogen. The scanning electron microscopy (SEM) images were captured with a Hitachi SU8010 microscope at 4 kV. The transmission electron microscopy (TEM) images were recorded on an FEI Tecnai G2 F30, which was operated at an accelerating voltage of 300 kV. The element distributions of the catalysts were detected by energy dispersive spectrometer (EDS) mapping. A PE Avio200 (America) inductively coupled plasma optical emission spectroscope (ICP-OES) was used to determine the elemental compositions. For ICP-OES analysis, a 20 mg sample was mixed with 2 mL concentrated nitric acid, 2 mL HF, and 0.5 mL H₂O₂. Furthermore, the mixture was treated at 80 °C in a graphite digestion apparatus under sealed conditions. After about 2 h, when the mixture became clear and transparent, it was diluted to the required concentration with H₂O. The ²⁷Al solid-state nuclear magnetic resonance (NMR) test was carried out on a Bruker AVANCE III HD 600 MHz spectrometer. The X-ray photoelectron spectra (XPS) were determined with a Thermo Fisher Scientific K-Alpha. The electron paramagnetic resonance (EPR) was analyzed with a JEOL JES-FA200 instrument at -196 °C. The ultraviolet-visible spectra (UV-vis) were determined with a Shimadzu UV 3600 spectrometer, and BaSO₄ was used as the reference sample.

The temperature-programmed desorption of NH₃ (NH₃-TPD) was measured by an MFTP-3060 chemisorption analyzer. First of all, a 100 mg catalyst was pretreated at 400 °C

in N₂ atmosphere for 1 h. After cooling to 30 °C and holding for 10 min, 4000 ppm NH₃ was injected into the sample for 30 min. Subsequently, the purging process was conducted at 100 °C with He gas for 1 h to remove physically adsorbed NH₃. After these steps were complete, the TPD profiles of NH₃ were obtained under a He atmosphere from 100 to 700 °C with a temperature ramp rate of 10 °C min⁻¹.

Additionally, to explore the reducibility of zeolite products, temperature-programmed reduction of hydrogen (H₂-TPR) was performed on an MFTP-3060 apparatus. To start with, a 100 mg catalyst was treated using the same purification method as NH₃-TPD, as described above. Then 5% H₂/He was introduced at a 30 mL min⁻¹ flow rate to establish a baseline. Eventually, the H₂-TPR profiles were obtained from 100 °C to 850 °C with a 10 °C min⁻¹ temperature ramp rate.

The in situ diffuse reflection infrared Fourier spectroscopy (DRIFTS) adsorption analyses under NH₃ were carried out on a Thermo Scientific Nicolet iS20 spectrometer with an in situ diffuse reflection cell equipped with KBr windows. Firstly, the catalysts were purified by N₂ at 400 °C for 1 h with a 50 mL min⁻¹ flow rate. Later, the catalysts were cooled to 100 °C to record the background spectra. To complete the NH₃ adsorption process, the catalysts were treated with NH₃ for 30 min. After that, the catalysts were purged for 1 h under N₂ conditions. The spectra were collected by accumulating 32 scans with a resolution of 4 cm⁻¹.

3.3. Catalytic Performance Tests

The NH₃-SCR catalytic experiments were performed in a fixed-bed reactor system with 100 mg (60–100 mesh) catalyst pellets, and the testing range was 150–400 °C. The catalysts were tested at a total flow rate of 400 mL min⁻¹, and the GHSV was 200,000 h⁻¹. Furthermore, the simulated test gases comprised 500 ppm NH₃, 500 ppm NO, 50 ppm SO₂ (when used), 5 vol% O₂, and 5 vol% H₂O, with the balance being N₂. The outlet gases were analyzed with a Thermo Scientific Nicolet Antaris IGS. The equations for calculating NO_x conversion, N₂, NO₂, and N₂O selectivity are as follows:

$$\text{NO}_x \text{ conversion} = \frac{[\text{NO}]_{\text{in}} - [\text{NO}]_{\text{out}} - [\text{NO}_2]_{\text{out}} - 2[\text{N}_2\text{O}]_{\text{out}}}{[\text{NO}]_{\text{in}}} \times 100\% \quad (1)$$

$$\text{N}_2 \text{ selectivity} = \frac{[\text{NH}_3]_{\text{in}} + [\text{NO}]_{\text{in}} - [\text{NH}_3]_{\text{out}} - [\text{NO}]_{\text{out}} - [\text{NO}_2]_{\text{out}} - 2[\text{N}_2\text{O}]_{\text{out}}}{[\text{NH}_3]_{\text{in}} + [\text{NO}]_{\text{in}} - [\text{NH}_3]_{\text{out}} - [\text{NO}]_{\text{out}}} \times 100\% \quad (2)$$

$$\text{NO}_2 \text{ selectivity} = \frac{[\text{NO}_2]_{\text{out}}}{[\text{NH}_3]_{\text{in}} + [\text{NO}]_{\text{in}} - [\text{NH}_3]_{\text{out}} - [\text{NO}]_{\text{out}}} \times 100\% \quad (3)$$

$$\text{N}_2\text{O selectivity} = \frac{2[\text{N}_2\text{O}]_{\text{out}}}{[\text{NH}_3]_{\text{in}} + [\text{NO}]_{\text{in}} - [\text{NH}_3]_{\text{out}} - [\text{NO}]_{\text{out}}} \times 100\% \quad (4)$$

where [NO]_{in} and [NH₃]_{in} indicate the concentrations of NO and NH₃ in the inlet gases, respectively, while [NH₃]_{out}, [NO]_{out}, [NO₂]_{out} and [N₂O]_{out} represent the concentrations of NH₃, NO, NO₂ and N₂O in the outlet gases, respectively.

4. Conclusions

The CuCe_x-SSZ-16 series catalysts modified with different amounts of Ce were synthesized via the ion-exchange process and measured under simulated NH₃-SCR conditions. The results reveal that the CuCe_{0.77}-SSZ-16 and CuCe_{0.87}-SSZ-16 catalysts have better low-temperature (<250 °C) NH₃-SCR performance and outstanding hydrothermal stability compared with Cu-SSZ-16. Meanwhile, the positive effects increase with an increase in the Ce contents, and the CuCe_{0.87}-SSZ-16 catalyst shows the best hydrothermal stability. In general, the introduction of 0.87 wt.% Ce effectively promotes the stability of the AFX framework and facilitates the formation of Cu²⁺-2Z species, which are beneficial to hydrothermal stability. Through a combination of multiple characterization techniques, the

effects of adding Ce were investigated. The PXRD results show that the AFX structure is retained in the hydrothermally treated sample with Ce, suggesting that adding Ce can stabilize the skeleton of the catalysts. The ^{27}Al MAS NMR results indicate that adding Ce may have increased the framework aluminum in the catalysts, resulting in better structural stability in the fresh and aged samples. Furthermore, the analyses of Cu species by XPS, EPR, H_2 -TPR, and in situ DRIFTS demonstrate that Ce ion exchange significantly increases the amount of Cu^{2+} -2Z species in the catalysts and reduces the formation of CuO_x , leading to good hydrothermal stability. Even after hydrothermal treatment at $800\text{ }^\circ\text{C}$, most of the framework aluminum and the majority of active Cu^{2+} -2Z species are retained in the aged catalysts with Ce additives, preventing a significant decrease in NH_3 -SCR activity. In conclusion, $\text{CuCe}_{0.87}$ -SSZ-16 shows remarkable NH_3 -SCR performance and outstanding hydrothermal stability and has great application prospects for NO_x removal.

Supplementary Materials: The following supporting information can be downloaded at <https://www.mdpi.com/article/10.3390/catal13040742/s1>. The synthesis of the catalysts. Figure S1: N_2 , NO_2 , and N_2O selectivity over Cu-SSZ-16, $\text{CuCe}_{0.77}$ -SSZ-16, and $\text{CuCe}_{0.87}$ -SSZ-16 before (a–c) and after hydrothermal treatment at $750\text{ }^\circ\text{C}$ (d–f) and $800\text{ }^\circ\text{C}$ (g–i). Figure S2: SEM images of Cu-SSZ-16-800HT (a,d), $\text{CuCe}_{0.77}$ -SSZ-16-800HT (b,e), and $\text{CuCe}_{0.87}$ -SSZ-16-800HT (c,f). Figure S3: Deconvolution of ^{27}Al NMR spectra over SSZ-16-Fresh, Cu-SSZ-16-Fresh, $\text{CuCe}_{0.77}$ -SSZ-16-Fresh, and $\text{CuCe}_{0.87}$ -SSZ-16-Fresh. Figure S4: XPS spectra of Cu 2p (a) and Ce 3d (b) over Cu-SSZ-16-800HT, $\text{CuCe}_{0.77}$ -SSZ-16-800HT, and $\text{CuCe}_{0.87}$ -SSZ-16-800HT. Figure S5: UV-vis spectra of Cu-SSZ-16-Fresh, $\text{CuCe}_{0.77}$ -SSZ-16-Fresh, and $\text{CuCe}_{0.87}$ -SSZ-16-Fresh. Figure S6: EPR spectra of Cu-SSZ-16-Fresh, $\text{CuCe}_{0.77}$ -SSZ-16-Fresh, and $\text{CuCe}_{0.87}$ -SSZ-16-Fresh. Figure S7: Deconvolution of in situ DRIFTS curves over Cu-SSZ-16-Fresh, $\text{CuCe}_{0.77}$ -SSZ-16-Fresh, and $\text{CuCe}_{0.87}$ -SSZ-16-Fresh.

Author Contributions: Conceptualization, Y.L. and J.J.; methodology, Z.L. and X.J.; formal analysis, Y.L., R.L. (Ruicong Liang) and Z.L.; investigation, R.L. (Rui Li) and R.L. (Ruicong Liang); data curation, Y.L. and R.L. (Rui Li); writing—original draft preparation, Y.L.; writing—review and editing, R.L. (Rui Li) and J.J.; supervision, J.J.; funding acquisition, J.J. All authors have read and agreed to the published version of the manuscript.

Funding: This research was funded by the National Natural Science Foundation of China (Grant No. 21971259).

Data Availability Statement: Data are available in the main text and the supplementary files.

Conflicts of Interest: The authors declare no conflict of interest.

References

1. Skalska, K.; Miller, J.; Ledakowicz, S. Trends in NO_x abatement: A review. *Sci. Total Environ.* **2010**, *408*, 3976–3989. [[CrossRef](#)] [[PubMed](#)]
2. Lasek, J.A.; Lajnert, R. On the Issues of NO_x as Greenhouse Gases: An Ongoing Discussion & hellip. *Appl. Sci.* **2022**, *12*, 10429. [[CrossRef](#)]
3. Zhang, X.Y.; Dou, T.T.; Wang, Y.; Yang, J.Y.; Wang, X.; Guo, Y.Y.; Shen, Q.; Zhang, X.; Zhang, S.Q. Green synthesis of Cu-SSZ-13 zeolite by seed-assisted route for effective reduction of nitric oxide. *J. Clean. Prod.* **2019**, *236*, 117667. [[CrossRef](#)]
4. Borfecchia, E.; Lomachenko, K.A.; Giordanino, F.; Falsig, H.; Beato, P.; Soldatov, A.V.; Bordiga, S.; Lamberti, C. Revisiting the nature of Cu sites in the activated Cu-SSZ-13 catalyst for SCR reaction. *Chem. Sci.* **2015**, *6*, 548–563. [[CrossRef](#)]
5. Fu, G.Y.; Yang, R.N.; Liang, Y.Q.; Yi, X.F.; Li, R.; Yan, N.N.; Zheng, A.M.; Yu, L.; Yang, X.B.; Jiang, J.X. Enhanced hydrothermal stability of Cu/SSZ-39 with increasing Cu contents, and the mechanism of selective catalytic reduction of NO_x . *Microporous Mesoporous Mater.* **2021**, *320*, 111060. [[CrossRef](#)]
6. Li, R.; Zhu, Y.J.; Zhang, Z.P.; Zhang, C.Q.; Fu, G.Y.; Yi, X.F.; Huang, Q.T.; Yang, F.; Liang, W.C.; Zheng, A.M.; et al. Remarkable performance of selective catalytic reduction of NO_x by ammonia over copper-exchanged SSZ-52 catalysts. *Appl. Catal. B Environ.* **2021**, *283*, 119641. [[CrossRef](#)]
7. Zhao, Z.C.; Yu, R.; Zhao, R.R.; Shi, C.; Gies, H.; Xiao, F.S.; De Vos, D.; Yokoi, T.; Bao, X.H.; Kolb, U.; et al. Cu-exchanged Al-rich SSZ-13 zeolite from organotemplate-free synthesis as NH_3 -SCR catalyst: Effects of Na^+ ions on the activity and hydrothermal stability. *Appl. Catal. B Environ.* **2017**, *217*, 421–428. [[CrossRef](#)]
8. Hernández-Salgado, G.I.; López-Curiel, J.C.; Fuentes, G.A. A Comparative Study of the NH_3 -SCR Activity of Cu/SSZ-39 and Cu/SSZ-13 with Similar Cu/Al Ratios. *Top. Catal.* **2022**, *65*, 1495–1504. [[CrossRef](#)]

9. Chokkalingam, A.; Chaikittisilp, W.; Iyoki, K.; Keoh, S.H.; Yanaba, Y.; Yoshikawa, T.; Kusamoto, T.; Okubo, T.; Wakihara, T. Ultrafast synthesis of AFX-Type zeolite with enhanced activity in the selective catalytic reduction of NO_x and hydrothermal stability. *RSC Adv.* **2019**, *9*, 16790–16796. [[CrossRef](#)]
10. Li, R.; Jiang, X.Q.; Lin, J.C.; Zhang, Z.P.; Huang, Q.T.; Fu, G.Y.; Zhu, Y.J.; Jiang, J.X. Understanding the influence of hydrothermal treatment on NH₃-SCR of NO_x activity over Cu_x-SSZ-16. *Chem. Eng. J.* **2022**, *441*, 136021. [[CrossRef](#)]
11. Gao, F.; Washton, N.M.; Wang, Y.; Kollár, M.; Szanyi, J.; Peden, C.H.F. Effects of Si/Al ratio on Cu/SSZ-13 NH₃-SCR catalysts: Implications for the active Cu species and the roles of Brønsted acidity. *J. Catal.* **2015**, *331*, 25–38. [[CrossRef](#)]
12. Guo, A.Q.; Xie, K.P.; Lei, H.R.; Rizzotto, V.; Chen, L.M.; Fu, M.L.; Chen, P.R.; Peng, Y.; Ye, D.Q.; Simon, U. Inhibition Effect of Phosphorus Poisoning on the Dynamics and Redox of Cu Active Sites in a Cu-SSZ-13 NH₃-SCR Catalyst for NO_x Reduction. *Environ. Sci. Technol.* **2021**, *55*, 12619–12629. [[CrossRef](#)]
13. Wu, Q.; Fan, C.; Wang, Y.; Chen, X.P.; Wang, G.M.; Qin, Z.X.; Mintova, S.; Li, J.H.; Chen, J.J. Direct incorporating small amount of Ce (III) in Cu-SAPO-18 catalysts for enhanced low-temperature NH₃-SCR activity: Influence on Cu distribution and Si coordination. *Chem. Eng. J.* **2022**, *435*, 134890. [[CrossRef](#)]
14. Chen, Z.; Fan, C.; Pang, L.; Ming, S.J.; Liu, P.; Li, T. The influence of phosphorus on the catalytic properties, durability, sulfur resistance and kinetics of Cu-SSZ-13 for NO_x reduction by NH₃-SCR. *Appl. Catal. B Environ.* **2018**, *237*, 116–127. [[CrossRef](#)]
15. Liu, K.; Yan, Z.D.; Shan, W.P.; Shan, Y.L.; Shi, X.Y.; He, H. Quantitative determination of the Cu species, acid sites and NH₃-SCR mechanism on Cu-SSZ-13 and H-SSZ-13 at low temperatures. *Catal. Sci. Technol.* **2020**, *10*, 1135–1150. [[CrossRef](#)]
16. Usui, T.; Liu, Z.D.; Ibe, S.; Zhu, J.; Anand, C.; Igarashi, H.; Onaya, N.; Sasaki, Y.; Shiramata, Y.; Kusamoto, T.; et al. Improve the Hydrothermal Stability of Cu-SSZ-13 Zeolite Catalyst by Loading a Small Amount of Ce. *ACS Catal.* **2018**, *8*, 9165–9173. [[CrossRef](#)]
17. Luo, J.Y.; Gao, F.; Kamasamudram, K.; Currier, N.; Peden, C.; Yezerets, A. New insights into Cu/SSZ-13 SCR catalyst acidity. Part I: Nature of acidic sites probed by NH₃ titration. *J. Catal.* **2017**, *348*, 291–299. [[CrossRef](#)]
18. Martini, A.; Borfecchia, E.; Lomachenko, K.A.; Pankin, I.A.; Negri, C.; Berlier, G.; Beato, P.; Falsig, H.; Bordiga, S.; Lamberti, C. Composition-driven Cu-speciation and reducibility in Cu-CHA zeolite catalysts: A multivariate XAS/FTIR approach to complexity. *Chem. Sci.* **2017**, *8*, 6836–6851. [[CrossRef](#)] [[PubMed](#)]
19. Zhang, R.Q.; McEwen, J.S.; Kollár, M.; Gao, F.; Wang, Y.L.; Szanyi, J.; Peden, C. NO Chemisorption on Cu/SSZ-13: A Comparative Study from Infrared Spectroscopy and DFT Calculations. *ACS Catal.* **2014**, *4*, 4093–4105. [[CrossRef](#)]
20. Paolucci, C.; Khurana, I.; Parekh, A.A.; Li, S.C.; Shih, A.J.; Li, H.; Di, I.; John, R.; Albarracin-Caballero, J.D.; Yezerets, A.; et al. Dynamic multinuclear sites formed by mobilized copper ions in NO_x selective catalytic reduction. *Science* **2017**, *357*, 898–903. [[CrossRef](#)]
21. Song, J.; Wang, Y.L.; Walter, E.D.; Washton, N.M.; Mei, D.H.; Kovarik, L.; Engelhard, M.H.; Proding, S.; Wang, Y.L.; Peden, C.; et al. Toward Rational Design of Cu/SSZ-13 Selective Catalytic Reduction Catalysts: Implications from Atomic-Level Understanding of Hydrothermal Stability. *ACS Catal.* **2017**, *7*, 8214–8227. [[CrossRef](#)]
22. Gao, F.; Szanyi, J. On the hydrothermal stability of Cu/SSZ-13 SCR catalysts. *Appl. Catal. A Gen.* **2018**, *560*, 185–194. [[CrossRef](#)]
23. Chen, J.L.; Peng, G.; Liang, T.Y.; Zhang, W.B.; Zheng, W.; Zhao, H.R.; Guo, L.; Wu, X.Q. Catalytic Performances of Cu/MCM-22 Zeolites with Different Cu Loadings in NH₃-SCR. *Nanomaterials* **2020**, *10*, 2170. [[CrossRef](#)] [[PubMed](#)]
24. Kim, Y.J.; Lee, J.K.; Min, K.M.; Hong, S.B.; Nam, I.-S.; Cho, B.K. Hydrothermal stability of CuSSZ13 for reducing NO_x by NH₃. *J. Catal.* **2014**, *311*, 447–457. [[CrossRef](#)]
25. Fickel, D.W.; D’Addio, E.; Lauterbach, J.; Lobo, R.F. The ammonia selective catalytic reduction activity of copper-exchanged small-pore zeolites. *Appl. Catal. B Environ.* **2011**, *102*, 441–448. [[CrossRef](#)]
26. Xie, J.L.; Jin, Q.Q.; Fang, D.; Ye, Y.L.; Hou, S.S.; Wang, X.H.; He, F. Effect of La/Ce modification over Cu based Y zeolite catalysts on high temperature selectivity for selective catalytic reduction with ammonia. *J. Clean. Prod.* **2022**, *362*, 132255. [[CrossRef](#)]
27. Wang, Y.; Li, G.G.; Zhang, S.Q.; Zhang, X.Y.; Zhang, X.; Hao, Z.P. Promoting effect of Ce and Mn addition on Cu-SSZ-39 zeolites for NH₃-SCR reaction: Activity, hydrothermal stability, and mechanism study. *Chem. Eng. J.* **2020**, *393*, 124782. [[CrossRef](#)]
28. Mao, J.W.; Xu, B.; Hu, Y.K.; Zhang, C.Y.; Meng, H.M. Effect of Ce metal modification on the hydrothermal stability of Cu-SAPO-34 catalyst. *J. Fuel Chem. Technol.* **2020**, *48*, 1208–1216. [[CrossRef](#)]
29. Deng, D.; Deng, S.J.; He, D.D.; Wang, Z.H.; Chen, Z.P.; Ji, Y.; Yan, G.P.; Hou, G.J.; Liu, L.C.; He, H. A comparative study of hydrothermal aging effect on cerium and lanthanum doped Cu/SSZ-13 catalysts for NH₃-SCR. *J. Rare Earth.* **2021**, *39*, 969–978. [[CrossRef](#)]
30. Li, R.; Liang, Y.Q.; Zhang, Z.P.; Huang, Q.T.; Jiang, X.Q.; Yang, R.N.; Yu, L.; Jiang, J.X. Understanding roles of Ce on hydrothermal stability of Cu-SSZ-52 catalyst for selective catalytic reduction of NO_x with NH₃. *Catal. Today* **2022**, *405–406*, 125–134. [[CrossRef](#)]
31. Fickel, D.W.; Lobo, R.F. Copper Coordination in Cu-SSZ-13 and Cu-SSZ-16 Investigated by Variable-Temperature XRD. *J. Phys. Chem. C* **2010**, *114*, 1633–1640. [[CrossRef](#)]
32. Shi, Y.J.; Li, Z.M.; Wang, J.L.; Zhou, R.X. Synergistic effect of Pt/Ce and USY zeolite in Pt-based catalysts with high activity for VOCs degradation. *Appl. Catal. B Environ.* **2021**, *286*, 119936. [[CrossRef](#)]
33. Chen, B.H.; Xu, R.N.; Zhang, R.D.; Liu, N. Economical Way to Synthesize SSZ-13 with Abundant Ion-Exchanged Cu⁺ for an Extraordinary Performance in Selective Catalytic Reduction (SCR) of NO_x by Ammonia. *Environ. Sci. Technol.* **2014**, *48*, 13909–13916. [[CrossRef](#)] [[PubMed](#)]

34. Prodinge, S.; Derewinski, M.A.; Wang, Y.L.; Washton, N.M.; Walter, E.D.; Szanyi, J.; Gao, F.; Wang, Y.L.; Peden, C. Sub-micron Cu/SSZ-13: Synthesis and application as selective catalytic reduction (SCR) catalysts. *Appl. Catal. B Environ.* **2017**, *201*, 461–469. [[CrossRef](#)]
35. Klinowski, J. Solid-state NMR studies of molecular sieve catalysts. *Chem. Rev.* **1991**, *91*, 1459–1479. [[CrossRef](#)]
36. Zhao, Y.Y.; Choi, B.C.; Kim, D. Effects of Ce and Nb additives on the de-NO_x performance of SCR/CDPF system based on Cu-beta zeolite for diesel vehicles. *Chem. Eng. Sci.* **2017**, *164*, 258–269. [[CrossRef](#)]
37. Liu, W.J.; Long, Y.F.; Liu, S.N.; Zhou, Y.Y.; Tong, X.; Yin, Y.J.; Li, X.Y.; Hu, K.; Hu, J.J. Promotional effect of Ce in NH₃-SCO and NH₃-SCR reactions over Cu-Ce/SCR catalysts. *J. Ind. Eng. Chem.* **2022**, *107*, 197–206. [[CrossRef](#)]
38. Zhao, S.; Huang, L.M.; Jiang, B.Q.; Cheng, M.; Zhang, J.W.; Hu, Y.J. Stability of Cu–Mn bimetal catalysts based on different zeolites for NO_x removal from diesel engine exhaust. *Chinese J. Catal.* **2018**, *39*, 800–809. [[CrossRef](#)]
39. Shan, Y.L.; Shi, X.Y.; Yan, Z.D.; Liu, J.J.; Yu, Y.B.; He, H. Deactivation of Cu-SSZ-13 in the presence of SO₂ during hydrothermal aging. *Catal. Today* **2019**, *320*, 84–90. [[CrossRef](#)]
40. Chen, L.; Li, J.H.; Ablikim, W.; Wang, J.; Chang, H.Z.; Ma, L.; Xu, J.Y.; Ge, M.F.; Arandiyani, H. CeO₂–WO₃ Mixed Oxides for the Selective Catalytic Reduction of NO_x by NH₃ Over a Wide Temperature Range. *Catal. Lett.* **2011**, *141*, 1859–1864. [[CrossRef](#)]
41. Zhang, Z.P.; Li, R.M.; Wang, M.J.; Li, Y.S.; Tong, Y.M.; Yang, P.P.; Zhu, Y.J. Two steps synthesis of CeTiO_x oxides nanotube catalyst: Enhanced activity, resistance of SO₂ and H₂O for low temperature NH₃-SCR of NO_x. *Appl. Catal. B Environ.* **2021**, *282*, 119542. [[CrossRef](#)]
42. Li, H.R.; Yi, X.F.; Miao, J.F.; Chen, Y.T.; Chen, J.S.; Wang, J.X. Improved Sulfur Resistance of COMMERCIAL V₂O₅-WO₃/TiO₂ SCR Catalyst Modified by Ce and Cu. *Catalysts* **2021**, *11*, 906. [[CrossRef](#)]
43. Chen, L.; Ren, S.; Jiang, Y.H.; Liu, L.; Wang, M.M.; Yang, J.; Chen, Z.C.; Liu, W.Z.; Liu, Q.C. Effect of Mn and Ce oxides on low-temperature NH₃-SCR performance over blast furnace slag-derived X supported catalysts. *Fuel* **2022**, *320*, 123969. [[CrossRef](#)]
44. Bie, X.; Jiao, K.; Gong, C.; Qu, B.; Liu, D.; Ma, S. The Role of Medium Acid Sites Tuned by Ce Adding in Moderate-Temperature NH₃-SCR. *Catal. Lett.* **2022**, *152*, 2270–2279. [[CrossRef](#)]
45. Vennestrøm, P.; Katerinopoulou, A.; Tiruvalam, R.R.; Kustov, A.; Moses, P.G.; Concepcion, P.; Corma, A. Migration of Cu Ions in SAPO-34 and Its Impact on Selective Catalytic Reduction of NO_x with NH₃. *ACS Catal.* **2013**, *3*, 2158–2161. [[CrossRef](#)]
46. Guan, B.; Jiang, H.; Peng, X.S.; Wei, Y.F.; Liu, Z.Q.; Chen, T.; Lin, H.; Huang, Z. Promotional effect and mechanism of the modification of Ce on the enhanced NH₃-SCR efficiency and the low temperature hydrothermal stability over Cu/SAPO-34 catalysts. *Appl. Catal. A Gen.* **2021**, *617*, 118110. [[CrossRef](#)]
47. Xiang, X.; Cao, Y.; Sun, L.; Wu, P.F.; Cao, L.; Xu, S.T.; Tian, P.; Liu, Z.M. Improving the low-temperature hydrothermal stability of Cu-SAPO-34 by the addition of Ag for ammonia selective catalytic reduction of NO_x. *Appl. Catal. A Gen.* **2018**, *551*, 79–87. [[CrossRef](#)]
48. Chen, Z.Q.; Liu, L.; Qu, H.X.; Zhou, B.J.; Xie, H.F.; Zhong, Q. Migration of cations and shell functionalization for Cu-Ce-La/SSZ-13@ZSM-5: The contribution to activity and hydrothermal stability in the selective catalytic reduction reaction. *J. Catal.* **2020**, *392*, 217–230. [[CrossRef](#)]
49. Nanba, T.; Masukawa, S.; Ogata, A.; Uchisawa, J.; Obuchi, A. Active sites of Cu-ZSM-5 for the decomposition of acrylonitrile. *Appl. Catal. B Environ.* **2005**, *61*, 288–296. [[CrossRef](#)]
50. Ma, Y.Y.; Li, Z.F.; Zhao, N.; Teng, Y.L. One-pot synthesis of Cu–Ce co-doped SAPO-5/34 hybrid crystal structure catalysts for NH₃-SCR reaction with SO₂ resistance. *J. Rare Earth.* **2021**, *39*, 1217–1223. [[CrossRef](#)]
51. Zhang, T.; Liu, J.; Wang, D.X.; Zhao, Z.; Wei, Y.C.; Cheng, K.; Jiang, G.Y.; Duan, A.J. Selective catalytic reduction of NO with NH₃ over HZSM-5-supported Fe–Cu nanocomposite catalysts: The Fe–Cu bimetallic effect. *Appl. Catal. B Environ.* **2014**, *148–149*, 520–531. [[CrossRef](#)]
52. Su, W.K.; Li, Z.G.; Peng, Y.; Li, J.H. Correlation of the changes in the framework and active Cu sites for typical Cu/CHA zeolites (SSZ-13 and SAPO-34) during hydrothermal aging. *PCCP* **2015**, *17*, 29142–29149. [[CrossRef](#)] [[PubMed](#)]
53. Ma, L.; Cheng, Y.S.; Cavataio, G.; McCabe, R.W.; Fu, L.X.; Li, J.H. Characterization of commercial Cu-SSZ-13 and Cu-SAPO-34 catalysts with hydrothermal treatment for NH₃-SCR of NO_x in diesel exhaust. *Chem. Eng. J.* **2013**, *225*, 323–330. [[CrossRef](#)]
54. Luo, J.Y.; Wang, D.; Kumar, A.; Li, J.H.; Kamasamudram, K.; Currier, N.; Yezerets, A. Identification of two types of Cu sites in Cu/SSZ-13 and their unique responses to hydrothermal aging and sulfur poisoning. *Catal. Today* **2016**, *267*, 3–9. [[CrossRef](#)]
55. Wang, A.; Arora, P.; Bernin, D.; Kumar, A.; Kamasamudram, K.; Olsson, L. Investigation of the robust hydrothermal stability of Cu/LTA for NH₃-SCR reaction. *Appl. Catal. B Environ.* **2019**, *246*, 242–253. [[CrossRef](#)]

Disclaimer/Publisher’s Note: The statements, opinions and data contained in all publications are solely those of the individual author(s) and contributor(s) and not of MDPI and/or the editor(s). MDPI and/or the editor(s) disclaim responsibility for any injury to people or property resulting from any ideas, methods, instructions or products referred to in the content.